Medium Effects in ρ-Meson Photoproduction

F. Riek[a], R. Rapp[a], T.-S. H. Lee[b], Yongseok Oh[a]

[a] *Cyclotron Institute and Physics Department, Texas A&M University, College Station, Texas 77843-3366, USA*
[b] *Physics Division, Argonne National Laboratory, Argonne, Illinois 60439, USA*

Abstract

We compute dilepton invariant mass spectra from the decays of ρ mesons produced by photon reactions off nuclei. Our calculations employ a realistic model for the ρ photoproduction amplitude on the nucleon which provides fair agreement with measured cross sections. Medium effects are implemented via an earlier constructed ρ propagator based on hadronic many-body theory. At incoming photon energies of 1.5–3 GeV as used by the CLAS experiment at JLAB, the average density probed for iron targets is estimated at about half saturation density. At the pertinent 3-momenta the predicted medium effects on the ρ propagator are rather moderate. The resulting dilepton spectra approximately agree with recent CLAS data.

Key words: photoproduction, ρ meson, in-medium properties
PACS: 21.65.Jk, 25.20.Lj, 14.40.Cs

1. Introduction

The investigation of hadron properties in hot and/or dense matter is of fundamental interest in the context of approaching the transition(s) into a chirally restored and/or deconfined plasma of quarks and gluons. Intriguing effects have been observed in dilepton spectra measured in high-energy heavy-ion collisions [1, 2], which are consistent with a strong broadening of the ρ-meson spectral function by about a factor of $\sim$3 in hot and dense hadronic matter [3, 4]. The medium modifications of the ρ are believed to be largely driven by the baryonic component of the medium. The rapid expansion of the fireball formed in heavy-ion reactions implies that the emission spectra encode a rather large range of temperatures and densities of the evolving medium. It is therefore desirable to test the medium effects in a static environment, such as provided by ground-state nuclei. Hadronic models predict appreciable medium effects in cold nuclear matter, e.g., an increase of the width of low-momentum ρ mesons at saturation density by a factor of 2–3 over its vacuum value [3]. Several experiments have recently been conducted to measure ρ production off nuclei, in both proton- [5] and photon-induced [6, 7, 8] reactions. In Ref. [5] a rather small dilepton signal for the ρ has been reported with a mass distribution compatible with a dropping mass, while Refs. [6] and [8] extracted a moderate broadening with little, if any, mass shift in $\pi^+\pi^-$ and e^+e^- mass spectra, respectively. An inherent feature of nuclear production experiments is that rather large projectile energies are required to supply the rest mass of the ρ. These impart an appreciable 3-momentum on the ρ meson relative to the nucleus which enhances the probability for decays outside the nucleus thus reducing the effective density probed by these experiments. Nevertheless, valuable constraints for cold nuclear matter effects and their 3-momentum dependence on existing models for in-medium ρ spectral functions can be expected.

As in heavy-ion reactions, dileptons are of special interest due to their negligible final-state interactions. However, the initial states in heavy-ion collisions and nuclear production experiments are quite different. In the former case, the simplifying assumption of a thermal heat bath can be made, while in the latter case a reliable description of the elementary production process is mandatory. The pertinent baseline reaction on a single nucleon,

Email addresses: friek@comp.tamu.edu (F. Riek), rapp@comp.tamu.edu (R. Rapp), lee@phy.anl.gov (T.-S. H. Lee), yoh@comp.tamu.edu (Yongseok Oh)

$\gamma N \to e^+ e^- N$, has been studied in several theoretical works [9, 10, 11, 12, 13]. Generally, the low-energy cross section is dominated by baryon resonance formation, while at photon energies of ∼1.5–2 GeV t-channel exchange processes are expected to take over. Applications to nuclear targets can be found in Ref. [11], where a schematic model for the production process has been implemented into a transport simulation for final-state interactions, as well as in Ref. [8] for the CLAS data [7, 8].

In the present work we combine a microscopic model for ρ photoproduction on the nucleon [12] with an in-medium ρ spectral function computed in hadronic many-body theory [14, 15]. The production model is largely based on meson/Pomeron exchange which properly accounts for the cross section above photon energies of 2 GeV. At lower energies, we supplement additional s-channel resonance excitations with parameters directly taken from the in-medium selfenergy of the ρ spectral function [3, 15]. This establishes consistency between the production process and in-medium effects, and leaves no additional free parameters for the resulting cross sections for ρ production and dilepton invariant-mass spectra.

In Sec. 2 the ρ photoproduction model on the nucleon is presented and checked against total cross sections and dilepton invariant-mass spectra for deuteron targets. In Sec. 3 we apply our model to dilepton spectra off nuclei utilizing the in-medium ρ spectral function at densities estimated from the decay kinematics corresponding to the incoming photon spectrum in the CLAS experiment. We finish with conclusions in Sec. 4.

2. ρ Photoproduction on the Nucleon

Our starting point is the photoproduction amplitude for $\gamma p \to e^+ e^- p$ developed by two of us [12]. It accounts for σ, f_2, 2π and Pomeron t-channel exchange as well as nucleon s- and u-channel pole contributions, and gives a good description of experimental cross sections at photon energies above ∼2 GeV, cf. the dotted line in Fig. 1. (A similar model in Ref. [10] employs a stronger σ-exchange, see Ref. [12, 16] for further comparison.) At smaller photon energies, as part of the photon beam used by CLAS at JLAB ($q_0 \simeq$ 1–3.5 GeV), baryon resonances are expected to become important [17]. Here we adopt the same set of resonances as used in Ref. [14] to describe total photoabsorption spectra (to constrain the in-medium ρ spectral function)

Resonance	m_B	$\Gamma_B^{\rm tot}$	$\Gamma_{\rho N}$	$\frac{f^2_{\rho N B}}{4\pi}$	Λ_B
$\Delta(1232)$	1232	120	N/A	16.2	700
$\Delta(1620)$	1620	145	35	2.1	700
$\Delta(1700)$	1700	300	110	2.5	1000
$\Delta(1905)$	1905	350	315	7.0	1200
$N(1440)$	1440	350	10	1.1	600
$N(1720)$	1720	200	100	4.16	600
$N(1520)$	1520	120	25	6.5	600
$N(2090)$	2090	414	150	1.0	1000

Table 1: Resonance parameters (columns 2, 5 and 6) used in the elementary photoproduction amplitude. The dimensionless coupling constants (all other quantities are in [MeV]) are fixed to reproduce the values for the total and partial vacuum on-shell widths (columns 3 and 4) as in Refs. [3, 15] (the cut-off values of Refs. [3, 15] are kept fixed).

summarized in Tab. 1.[1] Due to the rather large photon energies involved we employ relativistic interaction vertices defined by the following ρ-N-B Lagrangians:

$$\begin{aligned}
\mathcal{L}^{\frac{1}{2}\frac{1}{2}^+} &= \tfrac{f_{\rho BN}}{m_\rho}\bar\Psi_R\,\gamma_5\,\sigma^{\mu\nu}\,\tau_i\rho^i_{\mu\nu}\,\Psi_N \quad + h.c.\,,\\
\mathcal{L}^{\frac{1}{2}\frac{3}{2}^+} &= \tfrac{f_{\rho BN}}{m_\rho}\bar\Psi^\mu_R\,\gamma_5\,\gamma^\nu\,\tau_i\,\rho^i_{\mu\nu}\,\Psi_N \quad + h.c.\,,\\
\mathcal{L}^{\frac{1}{2}\frac{3}{2}^-} &= \tfrac{f_{\rho BN}}{m_\rho}\bar\Psi^\mu_R\,\gamma^\nu\,\tau_i\,\rho^i_{\mu\nu}\,\Psi_N \quad + h.c.\,,\\
\mathcal{L}^{\frac{3}{2}\frac{1}{2}^-} &= \tfrac{f_{\rho BN}}{m_\rho}\bar\Psi_R\,\sigma^{\mu\nu}\,T_i\,\rho^i_{\mu\nu}\,\Psi_N \quad + h.c.\,,\\
\mathcal{L}^{\frac{3}{2}\frac{3}{2}^+} &= \tfrac{f_{\rho BN}}{m_\rho}\bar\Psi^\mu_R\,\gamma_5\,\gamma^\nu\,T_i\,\rho^i_{\mu\nu}\,\Psi_N \quad + h.c.\,,\\
\mathcal{L}^{\frac{3}{2}\frac{3}{2}^-} &= \tfrac{f_{\rho BN}}{m_\rho}\bar\Psi^\mu_R\,\gamma^\nu\,T_i\,\rho^i_{\mu\nu}\,\Psi_N \quad + h.c.\,,
\end{aligned} \tag{1}$$

where $\sigma^{\mu\nu} = \frac{i}{2}[\gamma^\mu,\gamma^\nu]$, $\rho_i^{\mu\nu} = \partial^\mu\rho_i^\nu - \partial^\nu\rho_i^\mu$. Isospin, spin and parity of the resonance B are denoted by IJ^P, and τ_i, T_i are the usual isospin-1/2, $1/2 \to 3/2$ transition matrices.[2] As in Ref. [14], we utilize an improved version of the vector dominance model (VDM) [18, 19] which allows for a direct γ-N-B coupling and thus a better simultaneous description of hadronic and radiative decay widths (the γ-N-B coupling follows by replacing ρ_0^μ with A^μ in Eqs. (1); the parameter $r_B = 0.7$ [14] controls the deviation from naive VDM). The parameters (listed in Tab. 1) are adjusted to recover the same partial decay width for $B \to \rho N$ as the

[1] The ρNN formfactor has been reduced to 600 MeV improving consistency with Ref. [12], together with a 10% reduction of the ρ-N-$N(1720)$ coupling constant. The extra coupling to the $N(2090)$ increases the ρ production cross section around photon energies of ∼2 GeV by ∼15%.

[2] The spin-5/2 resonance is treated in a simplified way as in Ref. [14] via a $\frac{3}{2}\frac{3}{2}^+$ state with amended spin factor.

(updated) values in Ref. [3] (based on Ref. [14]), including monopole formfactors

$$F(|\vec{q}|) = \frac{\Lambda_{\rho BN}^2}{\Lambda_{\rho BN}^2 + \vec{q}^{\,2}} \tag{2}$$

with cutoff parameters $\Lambda_{\rho BN}$ [3]. The formfactors are consistently evaluated in the laboratory frame with $\vec{q}$ the three-momentum of the incoming photon (or ρ in the nuclear rest frame). The spin-1/2 and -3/2 baryon propagators are, respectively, taken as

$$\begin{aligned} S(q) &= \frac{\not{q} + m_B}{q^2 - m_B^2 + i\, m_B\, \Gamma_B}\,, \\ S^{\mu\nu}(q) &= \frac{\not{q} + m_B}{q^2 - m_B^2 + i\, m_B\, \Gamma_B}\, P^{\mu\nu}\,, \\ P^{\mu\nu} &= g^{\mu\nu} - \frac{1}{3}\gamma^\mu\,\gamma^\nu - \frac{2}{3}\frac{q^\mu q^\nu}{m_B^2} + \frac{1}{3}\frac{q^\mu\gamma^\nu - q^\nu\gamma^\mu}{m_B}\,, \end{aligned} \tag{3}$$

with masses m_B and total widths Γ_B as given in Tab. 1. We furthermore assume a linear increase of the in-medium resonance widths with density as in Refs. [3, 14]. We have verified that neglecting the momentum dependence of Γ_B in the propagators has an insignificant impact on our results. Including s- and u-channel graphs, the baryon resonance parts of the ρ-production amplitude take the form

$$\begin{aligned} \mathcal{M}_B^{\mu\nu} &= \chi_I\, \frac{\mu_B\, f_{\rho BN}}{2\, m_\rho} \bar{u}(p')\, [\Gamma_{VB}^\mu(k)\, S(p+q) \\ &\quad \times \Gamma_{\gamma B}^\nu(q) + \Gamma_{\gamma B}^\nu(q)\, S(p-k)\, \Gamma_{VB}^\mu(k)]\, u(p), \\ \mathcal{M}_B^{\mu\nu} &= \chi_I\, \frac{\mu_B\, f_{\rho BN}}{2\, m_\rho} \bar{u}(p')\, [\Gamma_{VB}^{\mu\alpha}(k)\, S_{\alpha\beta}(p+q) \\ &\quad \times \Gamma_{\gamma B}^{\nu\beta}(q) + \Gamma_{\gamma B}^{\nu\alpha}(q)\, S_{\alpha\beta}(p-k)\, \Gamma_{VB}^{\mu\beta}(k)\Big]\, u(p), \end{aligned} \tag{4}$$

for intermediate spin-1/2 and -3/2 states, respectively; p and p' are the momenta of the in- and outgoing nucleon, q (k) is the photon (ρ) momentum, and $\chi_I = 2$ (4/3) an isospin factor for $I = 1/2$ (3/2) resonances. The vertices Γ follow from Eq. (1):

$$\begin{aligned} \Gamma_{\gamma B}^\mu(q) &= \Gamma_{VB}^\mu(q) = 2\,\gamma_5\,\sigma^{\alpha\mu}\, q_\alpha\, F(\vec{q}), \\ \Gamma_{\gamma B}^{\mu\nu}(q) &= \Gamma_{VB}^{\mu\nu}(q) = (\gamma_5\,\gamma^\mu\, q^\nu - \gamma_5 \not{q}\, g^{\mu\nu})\; F(\vec{q}), \end{aligned} \tag{5}$$

for positive parity resonances and

$$\begin{aligned} \Gamma_{\gamma B}^\mu(q) &= \Gamma_{VB}^\mu(q) = 2\,\sigma^{\alpha\mu}\, q_\alpha\, F(\vec{q}), \\ \Gamma_{\gamma B}^{\mu\nu}(q) &= \Gamma_{VB}^{\mu\nu}(q) = (\gamma^\mu\, q^\nu - \not{q}\, g^{\mu\nu})\; F(\vec{q}), \end{aligned} \tag{6}$$

for negative parity resonances.

It is now straightforward to implement the production amplitude of Ref. [12], augmented by baryon resonances, into a mass differential cross section per nucleon for exclusive ρ and dilepton production. For the latter one obtains

$$\begin{aligned} &\left\langle \frac{d\sigma}{d\,M} \right\rangle_A (q, M) = \frac{m_N^2\, M}{(2\pi)^2\, \rho_A} \\ &\times \int \frac{d^3p}{(2\pi)^3} \frac{d^4k}{(2\pi)^4} \frac{d^4p'}{(2\pi)^4} \frac{e^2\, g^2}{(k^2)^2\, m_\rho^4} \frac{-\Im\, \Sigma_{\gamma\to e^+e^-}^{vac}(k)}{2\,\sqrt{(p\cdot q)^2}} \\ &\times \delta(k^2 - M^2)\, \delta(p'^{\,2} - m_N^2)\, \delta^4(q + p - k - p') \\ &\times \Theta\,(k_f - |\vec{p}\,|) \sum_{m_s, m_{s'}, \lambda} T^\mu(q,p,k)\; (T^\nu(q,p,k))^\dagger \\ &\times \left\{ P_{\mu\nu}^L(k)\, |G_\rho^L(k)|^2 + P_{\mu\nu}^T(k)\, |G_\rho^T(k)|^2 \right\}\,, \end{aligned} \tag{7}$$

where T^μ follows from summing $\mathcal{M}_i^{\mu\nu}$ over the photon polarization ϵ_μ in the elementary processes,

$$T^\mu(q,p,k) = \sum_{i\in\{\sigma,\phi,N,f_2,B\}} \mathcal{M}_i^{\mu\nu}(q,p,k)\, \epsilon_\nu(q)\,, \tag{8}$$

and the dilepton final state is represented by

$$\Im\, \Sigma_{\gamma\to e^+e^-}^{vac}(k) = -\frac{e^2\, k^2}{96\,\pi^2}\,. \tag{9}$$

Eq. (7) contains an average over the Fermi motion of the incoming nucleon ($p_0^2 = \vec{p}^{\,2} + m_N^2$) as needed for nuclear targets in the next section. Furthermore, $G_\rho^{L/T}$ denote the longitudinal and transverse components of the electromagnetic correlator [14] (in naive VDM, one has $G_\rho^{L/T} = (m_\rho^{(0)})^4/g_\rho^2 D_\rho^{L,T}$ where $D_\rho^{L,T}$ is the ρ propagator), and $P_{\mu\nu}^{L,T}$ are projection operators.

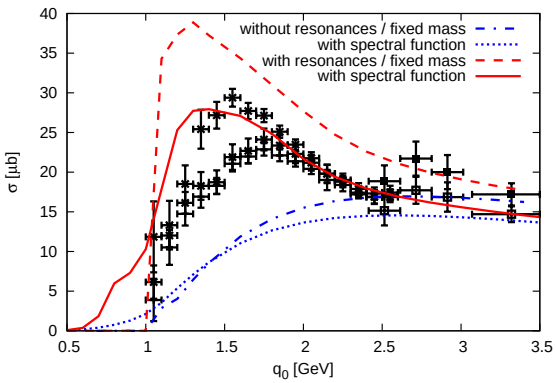

Figure 1: Total cross section for $\gamma\, p \to p\,\rho^0$ as a function of incident photon energy q_0 in the laboratory frame. The calculations are based on either a fixed ρ-mass of 770 MeV (dash-dotted and dashed line) or a full vacuum spectral function (dotted and solid line), either with (dashed and solid line) or without (dash-dotted and dotted line) baryon resonances. Data are from Refs. [23, 24].

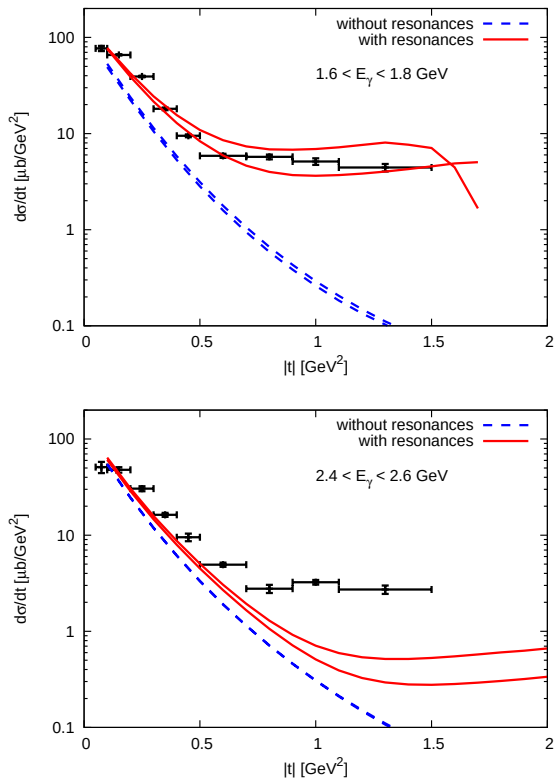

Figure 2: Differential ρ-meson photoproduction cross section. Calculations with (solid lines) and without (dashed lines) resonance contributions are compared to data [23], with 2 curves each representing the upper and lower end of the experimental photon energy window. In each case the full vacuum ρ-meson spectral function has been used.

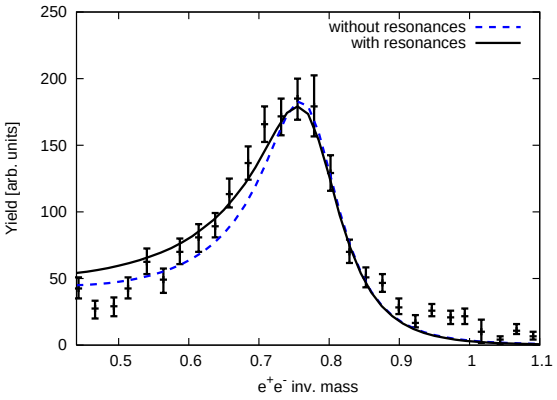

Figure 3: Dilepton invariant-mass spectrum for ρ photoproduction off deuterium with (solid line) and without (dashed line) baryon resonance contributions, compared to CLAS data after subtraction of ω and ϕ contributions [7, 8].

Our main interest in the present paper concerns the shape changes in the dilepton mass spectra induced by the in-medium ρ propagator encoded in $G_\rho^{L/T}$. Note, however, that Eq. (7) also accounts for the reduction in dilepton emission due to absorption of the ρ meson propagating in a nuclear medium at fixed density, via the in-medium reduction of $|G_\rho^{L/T}|^2$. For finite nuclei, this effect causes an appreciable decrease of the total e^+e^- production cross section, relative to a simple scaling with nuclear mass number, A (referred to as nuclear transparency ratio, T_A; see, e.g., Refs. [20, 21, 22] for the cases of ω and ϕ photoproduction).

We first test our production amplitude in the process $\gamma p \to \rho^0 p$. The photon-energy dependence of the ρ-production cross section is shown in Fig. 1. The contribution of the resonances nicely fills in low-energy strength that was missing in the original model of Ref. [12] and becomes negligible at energies beyond 2.5 GeV. Our calculations also illustrate that the inclusion of the free ρ width (as given by the vacuum spectral function of Ref. [14]) further improves the agreement with the low-energy cross section (however, in this region the extraction of the data is beset with significant model dependence [23]). The scattering-angle differential cross section (Fig. 2) reveals that the resonance excitations provide large contributions at large scattering angle which is supported by experiment.

Next we apply our model to dilepton invariant-mass spectra off deuterium. To mimic a finite nucleon-momentum distribution and rescattering effects in G_ρ we use a small average density of 0.1 ϱ_0 in Eq. (7) (folding over a realistic density distribution gives similar results). The incoming photon energies are weighted in 6 bins from q_0 = 1-3.5 GeV to simulate the Bremsstrahlungs-spectrum used by CLAS [25]. The shape of the e^+e^- spectra [8] is reasonably well reproduced, except for masses above 0.9 GeV where additional production processes might become relevant, see also Ref. [8].

3. Dilepton Spectra off Nuclei

To evaluate medium effects for nuclear targets, we first have to estimate the densities probed for a given nucleus. If the ρ meson were produced at rest, the density at its creation point would be a good approximation. However, since we are considering rather high photon energies the ρ meson will travel a significant distance before it decays. Based on the assumption that the (medium effect on the) ρ instantaneously adjusts to the surrounding medium,

the relevant density for the dilepton spectrum is the local density at the decay point, which we estimate as follows. For the incoming photon the interaction point is distributed according to a Woods-Saxon density profile (weighted by volume). The average travel distance of the ρ from its production to decay point is then calculated as

$$L = |\vec{v}|\,\gamma\,\tau, \qquad |\vec{v}| = |\vec{k}\,|\left(\vec{k}^{\,2} + m_\rho^2\right)^{-1/2}, \quad (10)$$

where $|\vec{v}|$ is the ρ three-velocity and τ its average lifetime (time dilated by a Lorentz γ factor). Under the present conditions, the latter is roughly $\sim 1\,\mathrm{fm/c}$ from the underlying in-medium spectral function, cf. Fig. 4. The velocity is estimated from the incoming photon energy for an on-shell ρ in the limiting case of forward production where the bulk of the differential cross section is concentrated (recall Fig. 2, where nuclear Fermi motion is neglected). The travel length L obtained in this way is then integrated over all production points resulting in the following distribution of decay points at a given density ϱ_x,

$$N(\varrho_x) = \int \varrho(r,0,\theta)\, r^2\, \sin(\theta)\, \delta(\varrho(r,L,\theta) - \varrho_x)\, d^3r,$$
$$\varrho(r,L,\theta) = \frac{\varrho_0}{1+\exp\left[\frac{(r^2+L^2-2\,r\,L\,\cos(\theta))^{1/2}-c}{z}\right]}, \quad (11)$$

with $z = 0.55$ fm and $c = 4.05$ fm for iron. At an average incoming photon energy of $\sim$2.1 GeV (representative for the CLAS experiment [25]) the average density at the decay point amounts to $0.5\,\varrho_0$. Varying the photon energy between 1.5 GeV and 2.5 GeV affects the average density by about $\pm 0.1\,\varrho_0$. We therefore display our dilepton spectra on iron for a density range of $\varrho_N = 0.4\text{-}0.6\,\varrho_0$.[3] Note that lower photon energies (probing larger densities) imply a smaller ρ-meson phase space which is therefore biased toward lower invariant masses. While the incoming photon energy spectrum is properly included at a given density via Eq. (7), the density-energy correlation is neglected. However, across the above range, the density variation of the dilepton spectra turns out to be quite moderate. A more accurate evaluation of this correlation should also include an exponential decay distribution of the ρ decays in L.

[3] This also reflects some of the uncertainty introduced by letting all ρ mesons decay after a fixed distance L, as compared to a distribution in L, since a different photon energy translates into a different L.

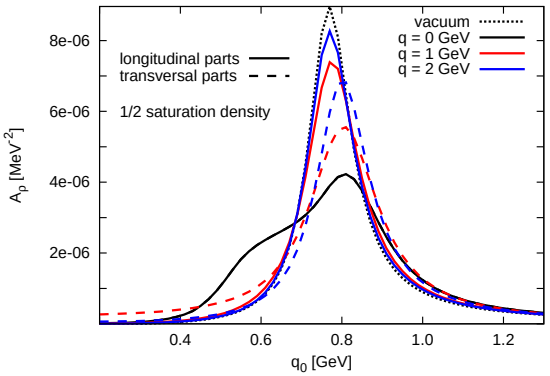

Figure 4: In-medium ρ-meson spectral function at various 3-momenta and nuclear density $0.5\,\varrho_0$ [15]; solid (dashed) lines: transverse (longitudinal) parts (identical at $q = 0$).

The main in-medium input to Eq. (7) is the ρ spectral function of Refs. [14, 15] which is displayed in Fig. 4 for transverse and longitudinal modes at various 3-momenta and at $\varrho_N = 0.5\,\varrho_0$. At 3-momenta relevant for CLAS ($q \simeq$ 1–2 GeV) the medium effects are significantly reduced compared to $q = 0$ (a consequence of the typical formfactor cutoffs, $\Lambda_{\rho BN} \simeq 0.6$ GeV; the reduction is more pronounced than, e.g., in the spectral function of Ref. [28] due to larger formfactor cutoffs used in there). In addition, a noticeable difference between longitudinal and transverse modes develops, the latter exhibiting an upward mass shift which is due to both pion cloud and P-wave resonance excitations. Note that in applications to dilepton spectra at CERN-SPS the in-medium spectral function is predominantly probed at 3-momenta below 1 GeV [15, 4]. This reiterates the notion that the CLAS data provide a novel test of the spectral function at high 3-momentum.

Our results for the dilepton invariant-mass spectra on iron are compared to the CLAS "excess" spectra in Fig. 5 using the density range as estimated above. For each density, the normalization is adjusted to the integrated strength of the data. Alternatively, one can determine the normalization by a least-square fit resulting in χ^2/N=1.29 (1.4) per data point (not) including the resonance contributions in the production process, compared to χ^2/N=1.34 (1.49) when normalizing to the data. In either case, the agreement with the data is fair (the in-medium broadening of the nucleon resonances has very little impact on the dilepton spectra). A slight discrepancy with the data for masses

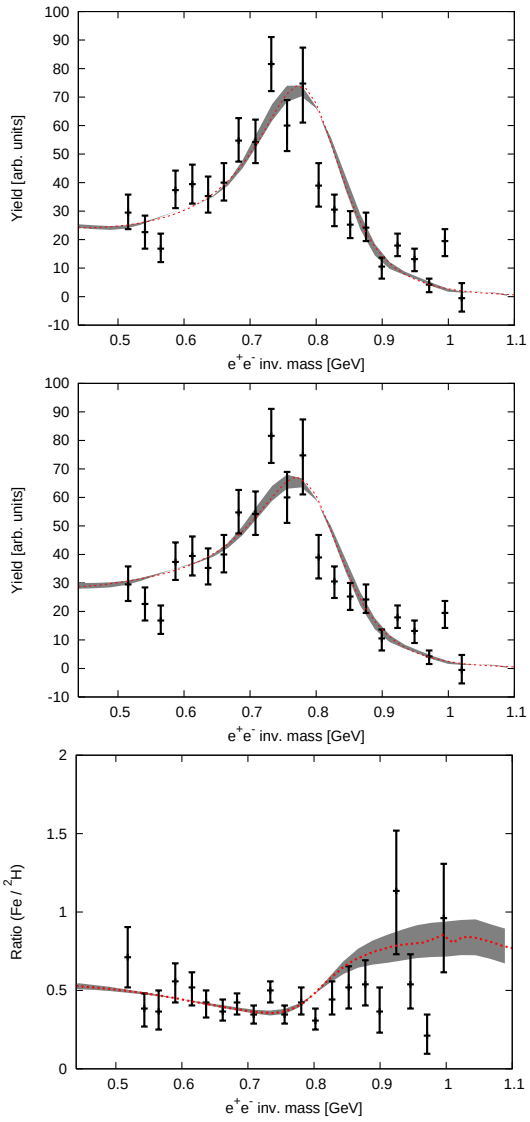

Figure 5: Theoretical calculations of dilepton spectra for photoproduction off iron compared to CLAS data [7, 8]. The bands represent the nuclear density range $\varrho_N = 0.4$–$0.6\ \varrho_0$. The curves in the upper (middle) panel are calculated without (with) baryon resonances (Tab. 1) in the elementary production amplitude, while the lower panel shows the iron-to-deuteron ratio for the full calculation.

of $M = 0.8$–0.85 GeV may allow for a small attractive mass shift of about -15 MeV.[4] Overall, the rather moderate medium effects in the (transverse and longitudinal parts of the) ρ spectral function at high 3-momentum (as seen in Fig. 4) are essentially in line with the CLAS spectra.[5] There are further effects which could modify our spectra at the several percent level, e.g., in-medium ω-meson decays along with interference/mixing with the ρ. σ and f_2 tadpole diagrams are not included in the spectral function; implementing the former with the coupling strength employed in the elementary production process [12] generates an attractive mass shift of about -10 MeV for the iron target. Further processes in inclusive production (e.g., $\gamma + N \to \rho + N + \pi$), additional resonance strength to accommodate large angle-scattering at high photon energies (recall lower panel in Fig. 2), or a more elaborate treatment of the baryon-resonance widths, might also play a role.

4. Conclusions

We have performed an essentially parameter-free calculation of ρ photoproduction off nuclei, combining a realistic model for the elementary production process with a hadronic many-body spectral function [15] which was extensively used before in the interpretation of dilepton spectra in heavy-ion collisions. An earlier constructed photoproduction amplitude [12] has been supplemented with resonance contributions as implicit in the in-medium ρ spectral function. A reasonable description of ρ photoproduction cross sections on the proton, as well as dilepton spectra on deuterium, emerged without major adjustments. The key test of the spectral function has been provided by the dilepton ("excess") spectra off iron. With average densities estimated from the decay kinematics for incoming photon energies as used at JLAB, the rather moderate in-medium effects reported by the CLAS experiment are fairly well reproduced. The main difference compared to the stronger effects observed in heavy-ion collisions is the rather large 3-momentum of the ρ in the CLAS data, for which the spectral function of Ref. [15] predicts a significantly reduced broadening. Clearly, a low-momentum cut on the dilepton spectra would enable a critical test of the predicted increase in medium effects. Further constraints could be obtained by analyzing absolute e^+e^- production cross sections (e.g., the so-called nuclear transparency ratio), as the in-medium spectral width of the ρ is directly related to its absorption in the nuclear medium.

[4] In the transport-based [29] Breit-Wigner fits in Ref. [8], the extracted ρ-mass is consistent with the free mass.

[5] The reduction of $\Lambda_{\rho NN}$ to 600 MeV entails an attraction of $\sim$15 MeV at $\varrho_N = \varrho_0$ in the transverse ρ spectral function.

Acknowledgments

The authors acknowledge useful discussions with C. Djalali. FR and RR were supported by a U.S. National Science Foundation CAREER grant No. PHY-0449489. TSHL was supported by the U.S. Department of Energy, Office of Nuclear Physics Division, under contract No. DE-AC02-06CH11357. YO was supported by the U.S. NSF under grants No. PHY-0457265, PHY-0758155 and the Welch Foundation under Grant No. A-1358.

Bibliography

[1] R. Arnaldi *et al.*, Phys. Rev. Lett. **96**, 162302 (2006).
[2] D. Adamova *et al.*, Phys. Lett. **B666**, 425 (2008).
[3] R. Rapp and J. Wambach, Adv. Nucl. Phys. **25**, 1 (2000).
[4] H. van Hees and R. Rapp, Nucl. Phys. **A806**, 339 (2008).
[5] M. Naruki *et al.*, Phys. Rev. Lett. **96**, 092301 (2006).
[6] G. M. Huber *et al.*, Phys. Rev. **C68**, 065202 (2003).
[7] R. Nasseripour *et al.*, Phys. Rev. Lett. **99**, 262302 (2007).
[8] M. H. Wood *et al.*, Phys. Rev. **C78**, 015201 (2008).
[9] M. Schafer, H. C. Donges, and U. Mosel, Phys. Lett. **B342**, 13 (1995).
[10] B. Friman and M. Soyeur, Nucl. Phys. **A600**, 477 (1996).
[11] M. Effenberger, E. L. Bratkovskaya, and U. Mosel, Phys. Rev. **C60**, 044614 (1999).
[12] Y.-s. Oh and T.S.H. Lee, Phys. Rev. **C69**, 025201 (2004).
[13] M. F. M. Lutz and M. Soyeur, Nucl. Phys. **A760**, 85 (2005).
[14] R. Rapp, M. Urban, M. Buballa, and J. Wambach, Phys. Lett. **B417**, 1 (1998).
[15] R. Rapp and J. Wambach, Eur. Phys. J. **A6**, 415 (1999).
[16] Y. Oh and H. Kim, Phys. Rev. **D68**, 094003 (2003).
[17] Y. Oh, C. M. Ko, and K. Nakayama, Phys. Rev. **C77**, 045204 (2008).
[18] N. M. Kroll, T. D. Lee, and B. Zumino, Phys. Rev. **157**, 1376 (1967).
[19] B. Friman and H. J. Pirner, Nucl. Phys. **A617**, 496 (1997).
[20] M. Kaskulov, E. Hernandez and E. Oset, Eur. Phys. J. A **31**, 245 (2007)
[21] M. Kotulla *et al.* [CBELSA/TAPS Collaboration], Phys. Rev. Lett. **100**, 192302 (2008)
[22] T. Ishikawa *et al.*, Phys. Lett. **B608**, 215 (2005).
[23] C. Wu *et al.*, Eur. Phys. J. **A23**, 317 (2005).
[24] ABBHHM-collaboration, Phys. Rev. **175**, 1669 (1968).
[25] C. Djalali, (CLAS) private comunications (2007).
[26] R. Erbe *et al.*, Phys. Rev. **188**, 2060 (1969).
[27] W. Struczinski *et al.*, Nucl. Phys. **B108**, 45 (1976).
[28] M. Post, S. Leupold, and U. Mosel, Nucl. Phys. **A741**, 81 (2004).
[29] P. Muhlich *et al.*, Phys. Rev. **C67**, 024605 (2003).